

Cite this: *Nanoscale*, 2012, **4**, 5102

www.rsc.org/nanoscale

PAPER

## Surface engineering of gold nanoparticles for *in vitro* siRNA delivery

Enyu Zhao,<sup>†a</sup> Zhixia Zhao,<sup>†a</sup> Jiancheng Wang,<sup>\*a</sup> Chunhui Yang,<sup>\*b</sup> Chengjun Chen,<sup>a</sup> Lingyan Gao,<sup>a</sup> Qiang Feng,<sup>a</sup> Wenjie Hou,<sup>a</sup> Mingyuan Gao<sup>\*b</sup> and Qiang Zhang<sup>a</sup>

Received 24th May 2012, Accepted 4th June 2012

DOI: 10.1039/c2nr31290e

Cellular uptake, endosomal/lysosomal escape, and the effective dissociation from the carrier are a series of hurdles for specific genes to be delivered both *in vitro* and *in vivo*. To construct siRNA delivery systems, poly(allylamine hydrochloride) (PAH) and siRNA were alternately assembled on the surface of  $11.8 \pm 0.9$  nm Au nanoparticles (GNP), stabilized by denatured bovine serum albumin, by the ionic layer-by-layer (LbL) self-assembly method. By manipulating the outmost PAH layer, GNP-PAH vectors with different surface electric potentials were prepared. Then, the surface potential-dependent cytotoxicity of the resultant GNP-PAH particles was evaluated *via* sulforhodamine B (SRB) assay, while the surface potential-dependent cellular uptake efficiency was quantitatively analyzed by using the flow cytometry method based on carboxyfluorescein (FAM)-labeled siRNA. It was revealed that the GNP-PAH particles with surface potential of +25 mV exhibited the optimal cellular uptake efficiency and cytotoxicity for human breast cancer MCF-7 cells. Following these results, two more positively charged polyelectrolytes with different protonating abilities in comparison with PAH, *i.e.*, polyethylenimine (PEI), and poly(diallyl dimethyl ammonium chloride) (PDDA), were chosen to fabricate similarly structured vectors. Confocal fluorescence microscopy studies indicated that siRNA delivered by GNP-PAH and GNP-PEI systems was better released than that delivered by the GNP-PDDA system. Further flow cytometric assays based on immunofluorescence staining of the epidermal growth factor receptor (EGFR) revealed that EGFR siRNA delivered by GNP-PAH and GNP-PEI exhibited similar down-regulation effects on EGFR expression in MCF-7 cells. The following dual fluorescence flow cytometry assays by co-staining phosphatidylserine and DNA suggested the EGFR siRNA delivered by GNP-PAH exhibited an improved silencing effect in comparison with that delivered by the commercial transfection reagent Lipofectamine 2000.

### Introduction

RNA interference (RNAi) is a post-transcriptional gene silencing mechanism mediated by small interfering RNA (siRNA), a 21–25 nucleotide (nt) double-stranded RNA molecule,<sup>1</sup> which can be incorporated into an RNA-induced silencing complex to induce the degradation of the target mRNAs in a sequence-specific manner.<sup>2,3</sup> Therefore, RNAi holds great promise in the therapy for different diseases.<sup>4,5</sup> However, siRNA molecules can hardly cross the cell membrane due to their large molecular size and negative charge.<sup>6,7</sup>

Different kinds of viral and non-viral methods have so far been developed for gene delivery purpose. Although the viral methods

based on recombinant viruses have achieved great progress in clinical trials, large scale production and host immunogenicity are challenges facing the viral methods.<sup>8,9</sup> In contrast, these problems can be solved by non-viral methods in spite of the fact that the levels of transfection and expression of delivered gene remain to be improved.<sup>10</sup> In this context, the cellular uptake, the endosomal/lysosomal escape, and the dissociation of siRNA from the gene carrier are important issues for improving the bioavailability of the loaded siRNA in designing effective vectors for both *in vitro* and *in vivo* applications.

Inorganic nanoparticles including gold,<sup>11–17</sup> iron oxide,<sup>18</sup> and quantum dots,<sup>19–22</sup> are being exploited as nonviral gene vectors recently, because the inorganic nanoparticles can effectively trap DNA or RNA and allow its escape from the endosome without degradation. Among them, gold nanoparticles (GNPs) have received increasing attentions owing to their excellent biocompatibility and low cytotoxicity.<sup>11,23–26</sup> Apart from forming covalent bonds with the reactive residues on the particle surface,<sup>14,15,27</sup> siRNA can facily be loaded onto the surface of GNPs *via* electrostatic attractions due to the polyionic nature of siRNA,<sup>13,17</sup> which is believed to be in favor of the subsequent

<sup>a</sup>State Key Laboratory of Natural and Biomimetic Drugs, School of Pharmaceutical Sciences, Peking University, Beijing, 100191, China. E-mail: wang-jc@bjmu.edu.cn; Fax: +86-10-82808683; Tel: +86-10-82808683

<sup>b</sup>Institute of Chemistry, Chinese Academy of Sciences, Beijing, 100190, China. E-mail: gaomy@iccas.ac.cn; Fax: +86-10-82613214; Tel: +86-10-82613214

<sup>†</sup> These authors contributed equally to this work.

release of the loaded siRNA in comparison with that covalently attached on the particle surface. In addition, the electrostatic attractions, as the typical driving force for the layer-by-layer (LbL) self-assembly techniques,<sup>28</sup> offer such a capacity that the surface potential of a particulate substrate can finely be tuned by the amount of the polyelectrolyte adsorbed on outmost surface, which provides a facile and effective measure for optimizing the cellular uptake efficiency which is strongly affected by surface potential of the particulate vectors.

Poly(allylamine hydrochloride) (PAH) is a widely used polyelectrolyte for constructing different types of LbL self-assembled films.<sup>29–31</sup> In the current study, it was used to sandwich siRNA on the surface of Au nanoparticles by the LbL self-assembling process, apart from finely tuning the surface potential of the resulting GNP-based siRNA vectors. In previous investigations, polyethylenimine (PEI) was adopted to develop such siRNA delivery vectors by alternately assembling siRNA and PEI on the surface of GNPs,<sup>13,32,33</sup> because the H<sup>+</sup> buffering PEI can enhance the endosomal Cl<sup>-</sup> accumulation and give rise to osmotic swelling and rupture of the endosomes, which is called the “proton-sponge” effect.<sup>32</sup> As a matter of fact, PEI is a branched polymer possessing primary amine (R–NH<sub>2</sub>), secondary amine (R<sub>2</sub>–NH), and tertiary amines (R<sub>3</sub>–N). Different from PEI, PAH only contains a primary amine in each repeating unit. Therefore, it is a suitable alternative model material for elucidating the impact of different parameters on the efficacy of GNP-based siRNA vectors constructed by co-assembling positively charged polyelectrolyte and negatively charged siRNA. In addition, it is much less cytotoxic than PEI.

In this work, PAH was used to assemble siRNA on the surface of GNPs of 11.8 nm. By tuning the amount of PAH on the outmost surface, the surface potential of the GNPs loaded with siRNA was effectively tuned, which allowed us to investigate the surface potential-dependent cytotoxicity and cellular uptake behavior of the resultant vectors. The endosomal/lysosomal escaping behavior of the GNP–PAH vector prepared under optimized conditions was also investigated by confocal fluorescence microscopy. To show the efficacy of the GNP–PAH vector in RNAi-mediated gene silencing, the epidermal growth factor receptor (EGFR) gene was chosen as a target for further *in vitro* experiments by using the GNP–PAH as EGFR siRNA carrier, and the results were then compared with those obtained by using commercial Lipofectamine 2000, GNP–PEI, and GNP–PDDA (poly(diallyl dimethyl ammonium chloride) as the EGFR siRNA vectors.

## Experimental

### Materials

PAH ( $M_w = 15$  kDa), PDDA ( $M_w = 100–200$  kDa), PEI ( $M_w = 25$  kDa), and sulforhodamine B were purchased from Sigma-Aldrich (St. Louis, MO). Bovine serum albumin (BSA) was purchased from Beijing Biodee Biotechnology Co., Ltd; Hoechst 33258 was purchased from Molecular Probes Inc. (Oregon, USA); OPTI-MEM, Rhodamine phalloidin and LysoTracker DND 99 (red) were purchased from Invitrogen (NY, USA); Agarose was purchased from GENE COMPANY (Hong Kong). Small interference RNA (sense strand: 5′-AGG AAU UAA

GAG AAG CAA CAU dTdT; antisense strand: 5′-AUG UUG CUU CUC UUA AUU CCU dTdT) targeting EGFR mRNA, a NC siRNA (sense strand: 5′-UUC UCC GAA CGU GUC ACG UdTdT; antisense strand: 5′-ACG UGA CAC GUU CGG AGA AdTdT), and FAM-labeled siRNA were purchased from Shanghai GenePharma (China).

### Preparation of citrate-stabilized Au nanoparticles

Briefly, 60 mL of 0.014% HAuCl<sub>4</sub> solution was prepared and heated to boiling. Then, 1.5 mL of a 1% trisodium citrate solution was introduced under vigorous stirring. After 10 min reflux, the reaction mixture was cooled down to room temperature for further use.

### Preparation of dBSA-coated Au nanoparticles

The dBSA was prepared by reducing BSA with NaBH<sub>4</sub>. In brief, 15 mL of aqueous solution containing 49.5 mg BSA was prepared and then 1.4 mg NaBH<sub>4</sub> was introduced. After being kept at room temperature under stirring for 1 h, the reaction mixture was transferred and then kept in a water bath at 70 °C for 20 min. The ligand exchange reaction was carried out by introducing 100 μL of the resultant dBSA solution into a 20 mL solution of the as-prepared Au nanoparticles. The dBSA-coated Au nanoparticles were collected after 24 h by centrifugation and then re-dispersed into water for further use.

### Preparation of GNP-based siRNA vectors

The GNP-based siRNA vectors were prepared by the LbL self-assembly method through the alternate depositions of negatively charged siRNA and positively charged polyelectrolyte such as PAH, PEI, PDDA. In detail, 1 mL dBSA-coated Au particle solution (3.66 nM) was firstly subjected to centrifugation at 16 000 × *g* for 15 min. After the supernatant was decanted, 1 mL of 1.0 mg mL<sup>-1</sup> PAH solution was introduced to re-disperse the dBSA-coated Au nanoparticles. After 30 min adsorption, the resultant crude Au@dBSA/PAH particles were collected by centrifugation at 16 000 × *g* for 15 min, and then re-dispersed in water. The resultant solution was subjected to centrifugation again to remove the non-adsorbed PAH. After that, the particle precipitate was dispersed by RNase-free water and the resultant dispersion was subjected to centrifugation at 5000 × *g* for 10 min to remove particle aggregates and the final concentration of Au@dBSA/PAH was adjusted to 1.00 nM. The concentration of the purified Au@dBSA/PAH was determined by absorption spectroscopy according to the absorbance at 525 nm. Then siRNA was introduced into the particle solution by an optimized molar ratio of 1500 : 1 to prepared Au@dBSA/PAH/siRNA. During the last step, different volumes of the PAH stock solution were introduced into aqueous dispersions of Au@dBSA/PAH/siRNA to produce Au@dBSA/PAH/siRNA/PAH vectors with different surface potentials.

By the same preparative procedures, the fluorescent GNP–PAH vectors with surface potentials of –25 mV, +15 mV, +25 mV, and +35 mV, GNP–PEI and GNP–PDDA with surface potential of +25 mV were prepared.

## Nanoparticle characterizations

The dBSA-coated Au particles were characterized with a transmission electron microscope (TEM) (JEM-100CXII) operating at an accelerating voltage of 100 kV. The hydrodynamic size and zeta potential of the composite particles, formed at different stages of the LbL self-assembly process, were determined on a Malvern Zetasizer Nano ZS instrument (Malvern, UK) equipped with a solid-state He–Ne laser ( $\lambda = 633$  nm).

## SRB assay

*In vitro* cytotoxicity of GNP–PAH vectors for MCF-7 cells was firstly analyzed by SRB assay. In brief, MCF-7 cells were seeded in 96-well plates at a density of 5000 cells per well. After 24 h proliferation, the cells were incubated at 37 °C with different formulations of NC siRNA in OPTI-MEM medium without antibiotics and serum. The final concentration of the siRNA was 50 nM, 100 nM, and 150 nM, respectively. After 6 h incubation, the culture medium was refreshed with RPMI-1640 medium supplemented with 10% FBS and 100 unit per mL penicillin and 100  $\mu\text{g mL}^{-1}$  streptomycin. After another 42 h incubation, the culture medium was carefully removed, and then 200  $\mu\text{L}$  of 10% trichloroacetic acid (TCA) was introduced into each well at 4 °C. After 1 h, the 96-well plate was rinsed by deionized water followed by air drying for 5 cycles. Subsequently, 100  $\mu\text{L}$  of SRB solution was added into each well and the staining was allowed for 30 min. After the SRB solution was removed, and the 96-well plate was rinsed using 1% acetic acid. After air drying, 200  $\mu\text{L}$  of 10 mM Tris base solution was added into each well to solubilize the protein-bound dye on a gyratory shaker for 30 min. The absorbance of the solution in each well was read on a microplate reader (BIO-RAD model 680, Bio-Rad Laboratories, Inc. Shanghai) at 540 nm.

## Cellular internalization efficacy

MCF-7 cells were seeded  $3.5 \times 10^5$  per well in a six-well plate. After 24 h proliferation, the PBS buffer solutions of GNP–PAH vectors with different surface potentials were introduced with final concentration of the FAM-labeled siRNA being around 100 nM. The following incubation was carried out at 37 °C in humidified air with 5%  $\text{CO}_2$ . After 3 h, the cells were harvested and washed three times with cold PBS and the cellular uptake of the fluorescent vectors was detected by a FACS Calibur flow cytometer (Becton Dickinson, San Jose, CA). The fluorescent siRNA–Lipofectamine 2000 and siRNA–PAH complexes were used as controls.

## Confocal fluorescence microscopy studies on the cellular internalization of the GNP–PAH vectors

Aliquots of  $3 \times 10^5$  MCF-7 cells were seeded in 35 mm dishes. After 24 h proliferation, the cells were incubated by the fluorescent GNP–PAH vectors of different surface potentials and their positive controls, *i.e.*, (FAM–siRNA)–Lipofectamine and (FAM–siRNA)–PAH, respectively, in the OPTI-MEM medium. The final concentration of siRNA was set to 100 nM. After 3 h incubation, the resulting cells were washed with cold PBS and then fixed by histiocyte stationary liquid (Saichi Biotech, Beijing)

at room temperature. Then they were sequentially stained by Rhodamine phalloidin for microfilament and Hoechst 33258 for cell nuclei, respectively. After thoroughly rinsed with PBS, the cells were subjected to confocal fluorescence microscopy analysis by Leica SP5 confocal microscope (Heidelberg) for showing the cellular internalization and sub-cellular distribution of the FAM-labeled siRNA.

## Endosomal/lysosomal escape of the GNP-based vectors

By similar procedures as mentioned above, the MCF-7 cells seeded in the 35 mm dishes were treated with fluorescent GNP–PAH, GNP–PEI, GNP–PDDA, siRNA–Lipofectamine, respectively. Then, LysoTracker DND 99 (red) with a concentration of 100 nM in PBS was used to stain the lysosomes at room temperature. Through the overlapping degree of the fluorescence from FAM-labeled siRNA and LysoTracker DND 99-labeled lysosomes, the endosomal/lysosomal escape was studied.

## Immunofluorescence assay on EGFR gene silencing

MCF-7 cells were firstly incubated in OPTI-MEM medium with GNP–PAH, GNP–PEI, GNP–PDDA, and Lipofectamine–siRNA, respectively. The concentration of siRNA was set to 100 nM and the incubation time was 6 h. Then the culture medium was refreshed with RPMI-1640 medium supplemented with 10% FBS and 100 unit per mL penicillin and 100  $\mu\text{g mL}^{-1}$  streptomycin. After another 72 h of incubation, the culture medium was carefully removed. After being washed with cold PBS, the cells were harvested through trypsinization and subjected to incubation firstly with 1% BSA for 30 min at room temperature, and with anti-EGFR rabbit monoclonal antibody (Abcam, Hong Kong) for 30 min at 37 °C. After being washed with PBS, the cells were stained by fluorescein isothiocyanate (FITC)-labeled goat anti-rabbit IgG at 37 °C for 1 h. By further fluorescence flow cytometry, the expression level of EGFR was measured.

## Cell apoptosis mediated by EGFR-siRNA

The MCF-7 cells obtained before the incubation with the anti-EGFR rabbit monoclonal antibody as mentioned above were subjected to double fluorescence staining using the annexin V-FITC Kit (Biosea, Beijing) containing both annexin V-FITC and propidium iodide. Then, the apoptosis of MCF-7 cells mediated by EGFR-siRNA was investigated by fluorescence flow cytometry.

## Results and discussion

### Preparation of Au@dBSA nanoparticles

The Au nanoparticles used herein for constructing the siRNA vectors were synthesized by reducing tetrachloroauric acid with sodium citrate. As shown in Fig. 1, the as-prepared GNPs are very uniform in shape. The average size is of  $11.8 \pm 0.9$  nm ( $n = 300$ ). It was demonstrated that the citrate-stabilized GNPs became colloiddally unstable in the presence of positively charged polyelectrolytes. Therefore, the chemically denatured bovine serum albumin (dBSA) was used to modify the GNPs to improve

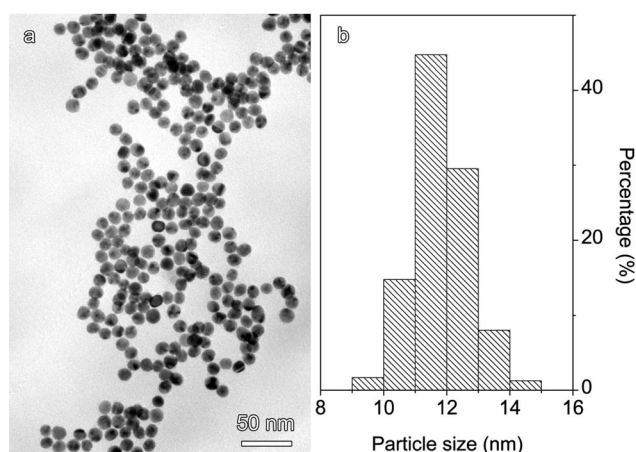
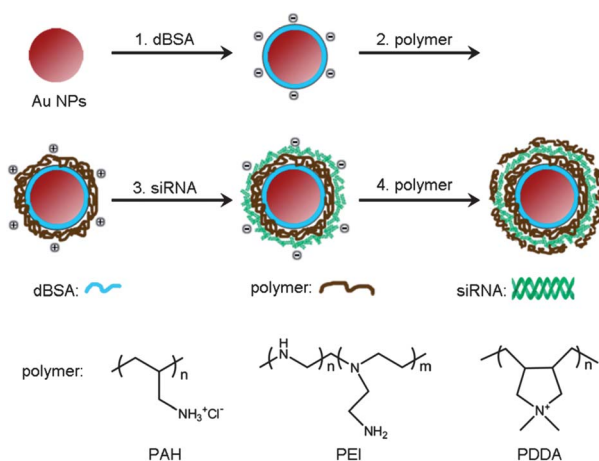


**Fig. 1** A representative transmission electron microscopy image of the as-prepared Au nanoparticles (a) together with the statistical size histogram of the particles (b).

their colloidal stability for surviving the LbL self-assembly process.<sup>34</sup> It is known that a BSA molecule possesses 1 free thiol group and 17 disulfide bonds. After being reduced by  $\text{NaBH}_4$ , the resultant dBSA carrying 35 thiol groups becomes a multi-dentate ligand suitable for capping the GNPs *via* its thiol groups. Due to the steric-hindrance effect, the dBSA-coated GNPs ( $\text{Au@dBSA}$ ) presented greatly improved colloidal stability in the presence of electrolytes and polyelectrolytes. Most importantly, the presence of numerous carboxyl groups makes the dBSA negatively charged polyelectrolyte around neutral pH, which enables the depositions of versatile positively charged species on the surface of the dBSA-coated GNPs, *via* the electrostatic attractions, for further engineering the particle surface.

### GNP-based siRNA vectors with different surface potentials

The depositions of the positively charged polyelectrolyte and negatively charged siRNA on  $\text{GNP@dBSA}$  were carried out according to a previous report,<sup>13</sup> except that no NaCl was introduced into the system. The whole process, as depicted in



**Scheme 1** Schematic illustration showing the preparation process of the GNP-based siRNA vectors together with chemical structures of positively charged polyelectrolytes, *i.e.*, PAH, PEI, and PDDA.

Scheme 1, was monitored by dynamic light scattering (DLS) and zeta potential measurements. The initial hydrodynamic size of dBSA-coated Au nanoparticles was determined to be 21.9 nm, while it was increased to 50.2 nm after one layer of PAH was deposited on the surface ( $\text{Au@dBSA/PAH}$ ). The following adsorption of siRNA further increased the hydrodynamic size to 64.1 nm for  $\text{Au@dBSA/PAH/siRNA}$ . Accompanying these changes, the zeta potential was changed from  $-25.5$  mV for  $\text{Au@dBSA}$  to  $+28.0$  mV for  $\text{Au@dBSA/PAH}$ , and then to a negative potential of  $-30.8$  mV after the siRNA layer was deposited. According to the UV-Vis spectroscopy analysis, there were approximately 1170 siRNA molecules deposited on each GNP. In general, the changes in both hydrodynamic size and zeta potential of the GNPs have good consistency, which strongly supports that the designed structure as shown in Scheme 1 has been achieved. To further tune the zeta potential of the vector particles, different amounts of PAH were deposited as the topmost layer following the adsorption of siRNA by varying the concentration of PAH in the system. In this way, the surface potential of the resultant vectors, denoted as  $\text{GNP-PAH}$ , was effectively tuned from negative potential up to  $+39.9$  mV when the concentration of PAH was raised to  $10 \mu\text{g mL}^{-1}$ , as shown in Fig. 2.

### Cytotoxicity of the GNP-PAH vectors

The surface electric potential is known to be strongly associated with the cytotoxic effects of nanoparticles. To show the surface potential-dependent cytotoxicity, a series of samples with zeta potentials of around  $-25$  mV ( $\text{GNP-PAH-1}$ ),  $+15$  mV ( $\text{GNP-PAH-2}$ ),  $+25$  mV ( $\text{GNP-PAH-3}$ ), and  $+35$  mV ( $\text{GNP-PAH-4}$ ), respectively, were prepared according to the tendency shown in Fig. 2. The cytotoxicity profiles of the  $\text{GNP-PAH}$  vectors for human breast cancer MCF-7 cells were evaluated *via* the sulforhodamine B (SRB) assays.<sup>35</sup> Two additional samples were prepared and used as the control. The first one was a siRNA-PAH complex in which the amount of siRNA was the same as those used for preparing the  $\text{GNP-PAH}$  vectors, while the amount of PAH was identical to that used for preparing

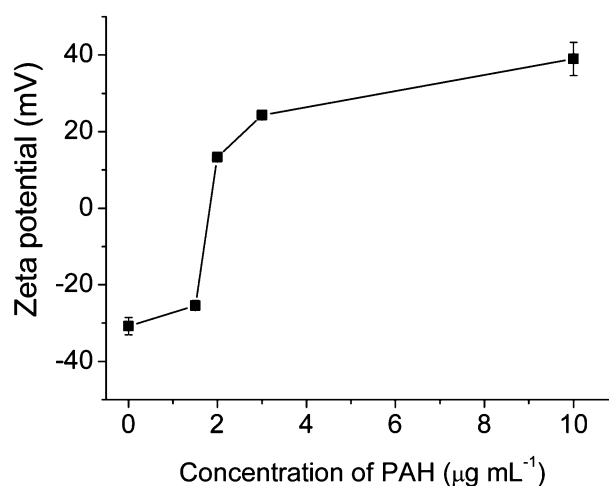


**Fig. 2** Zeta-potential of  $\text{Au@dBSA/PAH/siRNA/PAH}$  against the concentration of PAH used for depositing the outermost PAH layer.

GNP-PAH-3. The second one was siRNA-Lipofectamine 2000 (siRNA-Lipo) complex with an identical amount of siRNA encapsulated. The amount of Lipofectamine 2000 reagent was set according to its optimal ratio to siRNA. In this way, the cytotoxicity of different systems was evaluated according to the concentration of siRNA loaded. Detailed results shown in Fig. 3 suggest that when the concentration of siRNA is 50 nM, no significant difference is presented among all systems. When it is increased to 100 nM, siRNA-PAH and GNP-PAH-1 present decreased cell viabilities.

Upon further increase of the siRNA concentration to 150 nM, the cell viability of GNP-PAH-4 dramatically decreases and becomes the lowest, while that of GNP-PAH-3 remains the highest. According to these results, the GNP-PAH vector with the surface potential of +25 mV possesses the lowest cytotoxicity and it is almost nontoxic to MCF-7 cells when the concentration of siRNA is below 150 nM.

### Cellular uptake of the GNA-PAH vectors

It is well-known that the surface potential of nanoparticles is also strongly correlated to their cellular uptake behavior. To investigate this effect, fluorescent GNP-PAH-1 (-25 mV), GNP-PAH-2 (+15 mV), GNP-PAH-3 (+25 mV), and GNP-PAH-4 (+35 mV) were prepared by using carboxyfluorescein (FAM)-labeled siRNA. For comparison, fluorescent counterparts of siRNA-Lipofectamine 2000 and siRNA-PAH were also prepared and used as controls. The flow cytometry analysis on the MCF-7 cells incubated with all the above-mentioned samples respectively reveals that the fluorescence intensities of GNP-PAH groups fall almost between those of siRNA-Lipofectamine and siRNA-PAH, as shown in Fig. 4, following an order of siRNA-Lipofectamine 2000 (siRNA-Lipo) > GNP-PAH-3 > GNP-PAH-4 > GNP-PAH-2 > siRNA-PAH ~ GNP-PAH-1 > control (cells were not treated with any siRNA vectors). In

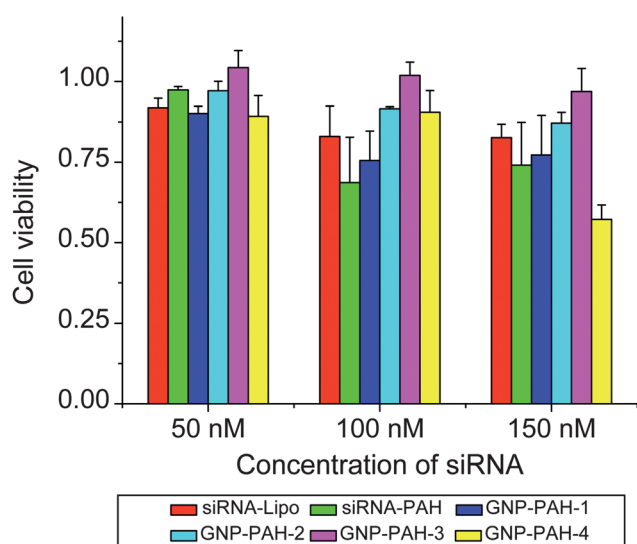


**Fig. 3** Viabilities of MCF-7 cells after being treated with siRNA-Lipofectamine 2000 (siRNA-Lipo), siRNA-PAH complex (siRNA-PAH), and the GNP-based vectors loaded with irrelevant siRNA (GNP-PAH-1, GNP-PAH-2, GNP-PAH-3, and GNP-PAH-4), respectively.

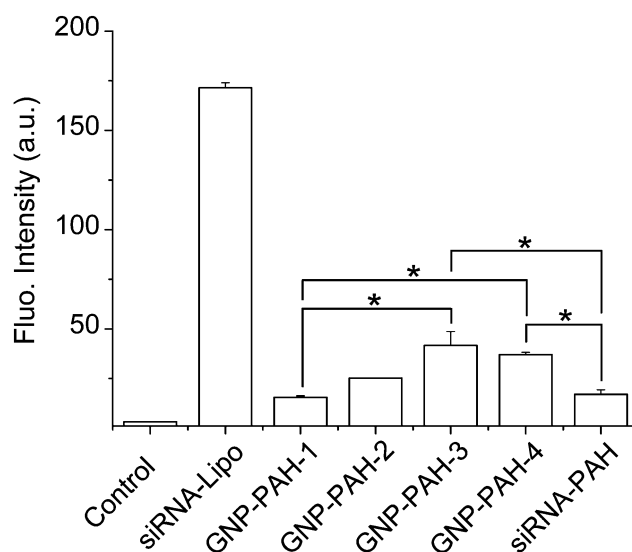


**Fig. 4** Cellular uptake efficiencies of the GNP-PAH vectors by MCF-7 cells characterized by the fluorescence flow cytometric analysis by using FAM-labeled siRNA ( $n = 2$ ,  $*p < 0.05$ ).

addition, the cellular uptake efficiencies of GNP-PAH vectors exhibit a surface potential-dependent non-monotonic behavior by showing a maximum at +25 mV.

To visualize the internalization of the GNP-PAH vectors and their following intracellular distributions, confocal fluorescence microscopy studies were carried out. The results shown in Fig. 5 suggest that GNP-PAH-1 hardly enters the MCF-7 cells (Fig. 5a). In contrast, when the surface potential is inverted to positive, the GNP-PAH vector gains the ability to enter the MCF-7 cells and shows the most remarkable internalization effect when the surface potential is increased to  $\sim +25$  mV (Fig. 5c), leading to an even distribution of the siRNA exclusively in the cytoplasm, quite comparable to that achieved by using siRNA-Lipofectamine 2000 (Fig. 5e). In principle, the cationic nanoparticles are more effective in binding with anionic mammalian cells. However, when the surface potential of GNP-PAH vector is raised to +35 mV, the cellular internalization efficiency is significantly lowered (Fig. 5d). The intracellular distribution of siRNA molecules is also altered by forming bigger aggregates, similar to that shown in the siRNA-PAH system (Fig. 5f). In the meantime, the siRNA complexes become localized not only in the cytoplasm but also on the membranes. In addition, the appearances of quite obvious disruption of the actin cytoskeleton and overall cell damage strongly support the higher toxicity introduced by ultrahigh positive surface potential.

All above-mentioned experimental results suggest that the surface potential of +25 mV is the optimal value balancing cytotoxicity and cellular uptake efficiency well for constructing the GNP-PAH vector. Therefore, GNP-PAH-3 was mainly used for the following investigations on endosomal/lysosomal escape and the gene silencing effect as well.

### Endosomal/lysosomal escape

To investigate the endosomal/lysosomal escape of the GNP-PAH vector, further confocal fluorescence microscopy studies

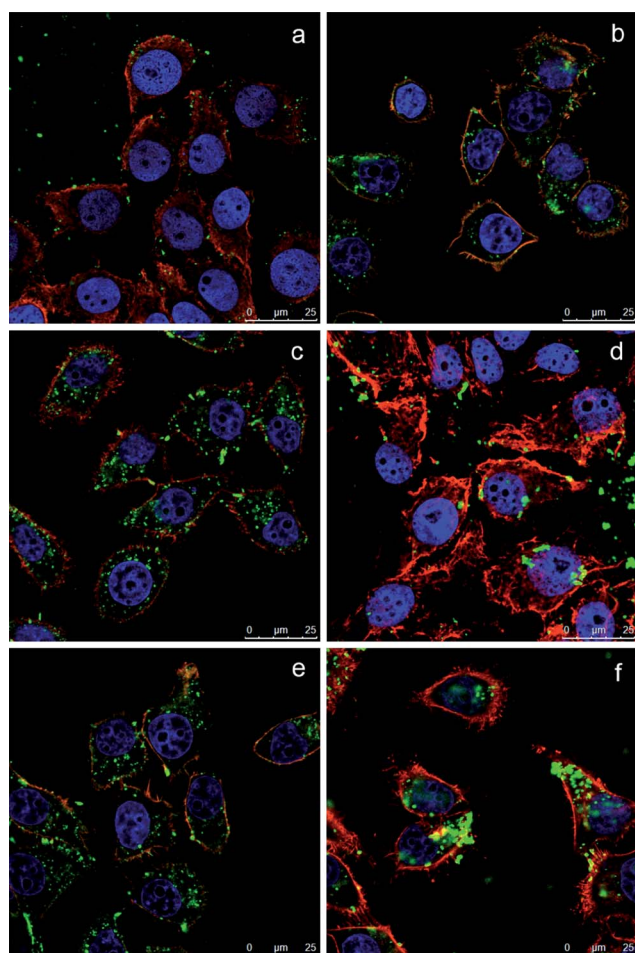


**Fig. 5** Confocal fluorescence microscopy images of MCF-7 cells treated with GNP-PAH-1 (a), GNP-PAH-2 (b), GNP-PAH-3 (c), GNP-PAH-4 (d), FAM-labeled siRNA-Lipofectamine 2000 (e), and FAM-labeled siRNA-PAH (f), respectively. The cell nuclei were stained with Hoechst 33258 (blue), and the cell membrane was stained with Rhodamine phalloidin (red). The FAM-labeled siRNA appear in green.

were carried out by labeling lysosome with a lysosomal marker LysoTracker Red DND-99 which emits red color fluorescence in contrast to FAM which emits green light on siRNA. Therefore, the correlation between the fluorescence localizations of siRNA and lysosome was used to investigate the endosomal/lysosomal escape. For showing the effect of molecular structure of the positively charged polyelectrolyte on the endosomal/lysosomal escape, PEI and PDDA were also used to replace PAH to prepare GNP-based siRNA vectors, denoted as GNP-PEI (Au@dBSA/PEI/siRNA/PEI) and GNP-PDDA (Au@dBSA/PDDA/siRNA/PDDA), respectively. The surface potentials of GNP-PEI and GNP-PDDA were tuned carefully to +25 mV to eliminate the surface potential-related effects.

The results shown in Fig. 5 reveal that the treatment of MCF-7 cells by GNP-PAH-3 leads to fluorescence patterns comprised of uniformly distributed tiny spots in the cytoplasm, similar to that obtained by using Lipofectamine 2000. The results shown in Fig. 6 further demonstrate that the co-localization of green and red fluorescence is the major occurrence for cells treated with

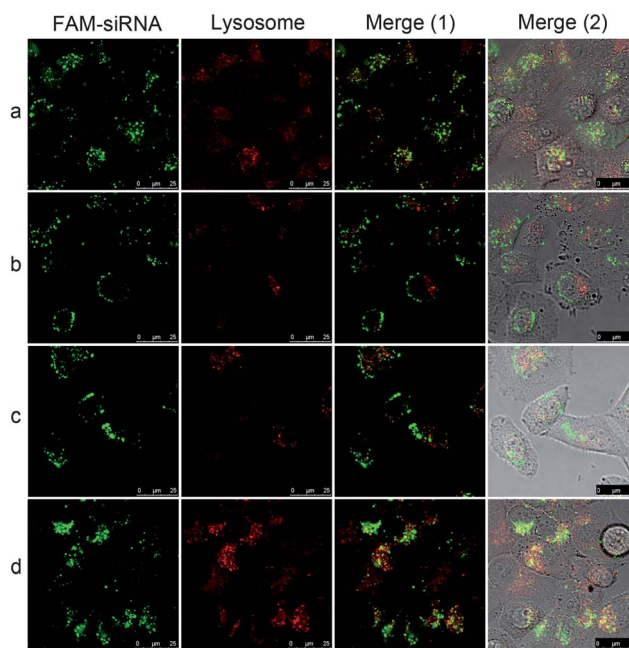


**Fig. 6** Confocal fluorescence microscopy images of MCF-7 cells treated with siRNA-Lipofectamine 2000 (row a), GNP-PAH-3 (row b), GNP-PEI (row c), and GNP-PDDA (row d), respectively. The lysosomes stained by LysoTracker Red DND-99 appear red while siRNA labeled by FAM appear green.

Lipofectamine 2000 (row a) and GNP-PDDA (row d), respectively. In contrast, such co-localization becomes greatly suppressed with respect to the cells treated with GNP-PAH-3 (row b) and GNP-PEI (row c), respectively, which suggests that GNP-PAH and GNP-PEI are superior to Lipofectamine and GNP-PDDA with respect to endosomal/lysosomal escape. These differences can be understood as follows. In fact, PEI is a branched polymer possessing primary amine ( $R-NH_2$ ), secondary amine ( $R_2-NH$ ), and tertiary amine ( $R_3-N$ ). In previous investigations, the “proton sponge” effect associated with the protonation of these groups was used to explain the escape of the PEI-based gene vector from the endosomes/lysosomes,<sup>32,36</sup> which should also be applicable for explaining the superior endosomal/lysosomal escape behavior of GNP-PAH vector as PAH has one primary amine group in each repeat unit. In contrast, the N atom in PDDA occurs as a quaternary ammonium salt ( $R_4-N^+$ ) and cannot be protonated to activate the proton sponge effect, therefore the GNP-PDDA vectors get heavily trapped in the lysosomes after cellular uptake. Although PEI- and PAH-based GNP vectors present similar endosomal/lysosomal escape abilities, PEI, PAH, and PDDA present different cytotoxicities. As shown in Fig. 7, PDDA is the most cytotoxic among these three polyelectrolytes with half maximal inhibitory concentration ( $IC_{50}$ ) around  $0.55 \mu g mL^{-1}$ . The  $IC_{50}$  value of PEI is an order of magnitude higher reaching  $5.6 \mu g mL^{-1}$ . In contrast, PAH is nearly non-cytotoxic. It is worth mentioning that further SRB assays revealed that no significant difference in cytotoxicity was observed among GNP-PAH-3, GNP-PEI (+25 mV), and GNP-PDDA (+25 mV) when the concentration of siRNA loaded in corresponding vectors was below 150 nM, which suggests that the cytotoxicity of the

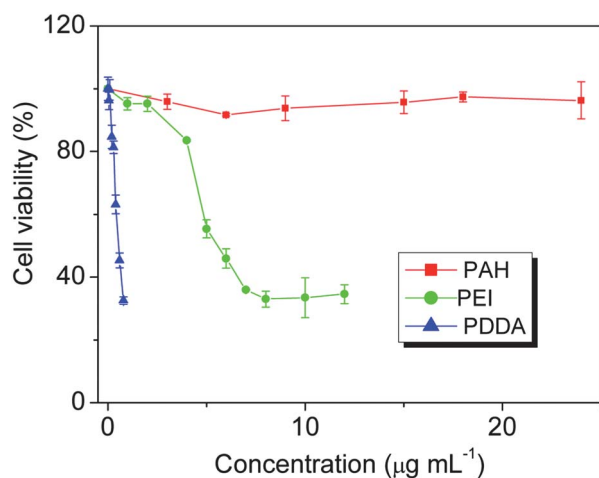


**Fig. 7** MCF-7 cell viabilities determined in the presence of PAH, PEI, and PDDA, respectively, by SRB assays.

positively charged polyelectrolytes is greatly suppressed after being assembled on the surface of GNPs.

### EGFR gene silencing

Epidermal growth factor receptor (EGFR), used as a model therapeutic target in the following experiments, is a membrane tyrosine kinase over-expressed in a large variety of solid tumors. EGFR is strongly associated with cell proliferation, decreased apoptosis, and enhanced metastasis.<sup>37,38</sup> Therefore, silencing EGFR by RNA interference may offer an alternative choice to anti-EGFR therapeutic strategy by inducing cell cycle arrest, apoptosis, and tumor cell growth inhibition.<sup>39–42</sup> To this end, the flow cytometric immunofluorescence assays on the EGFR protein expression levels in MCF-7 cells were carried out after they were treated with different vectors carrying EGFR siRNA. The results shown in Fig. 8 reveal that the EGFR expression level in MCF-7 cells pre-treated with different vectors follows the order of GNP-PEI (38.3% inhibition)  $\sim$  GNP-PAH-3 (36.9% inhibition)  $>$  siRNA-Lipofectamine 2000 (25.1% inhibition)  $>$  GNP-PDDA (16.9% inhibition). In addition, nearly no gene expression knockdown activity was observed from the MCF-7 cells treated with negative control (NC) siRNA.

Further flow cytometric analysis on the apoptosis of MCF-7 cells induced by EGFR siRNA was carried out *via* a double staining method by using fluorescein isothiocyanate (FITC) conjugated annexin V and propidium iodide (PI). Detailed results are shown in Fig. 9. The control cells that were not treated with any siRNA present a cell apoptosis rate of 4.20% (Fig. 9a), while the cells induced by NC siRNA carried by Lipofectamine 2000 (Fig. 9b) and GNP-PAH-3 (Fig. 9c) present similar apoptosis rates of 5.94% and 5.17%, respectively. In contrast, a relatively higher apoptosis rate of 9.96% is presented by the cells treated with the complex formed by PAH and NC siRNA, which suggests that the siRNA-PAH complex has certain cytotoxicity and explains the highest apoptosis rate of 15.93% achieved by the complex of (EGFR siRNA)-PAH (Fig. 9g). Since GNP-PAH-3 loaded with NC siRNA presents a low apoptosis rate of 5.17%, it can be deduced that the cytotoxicity of siRNA-PAH complex is suppressed if it is assembled on the surface of Au nanoparticles.

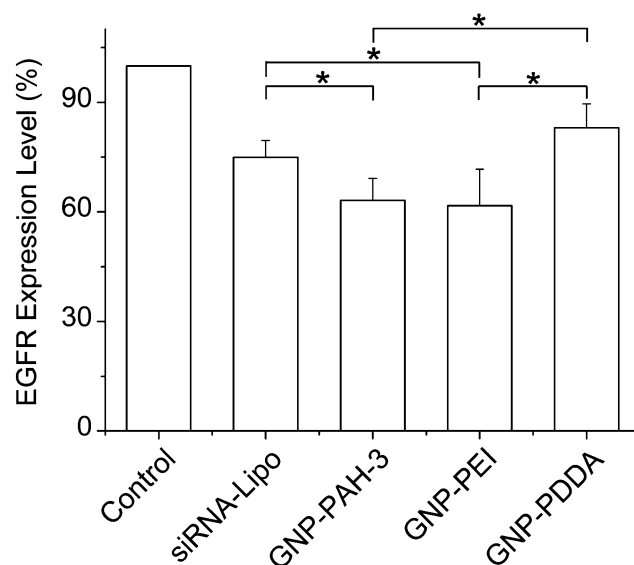


**Fig. 8** Flow cytometric immunofluorescence assay on EGFR expression levels in MCF-7 cells treated with siRNA-Lipofectamine 2000 (siRNA-Lipo), GNP-PAH-3, GNP-PEI, and GNP-PDDA vectors loaded with EGFR siRNA, respectively (\* $p < 0.05$ ). The EGFR expression level in MCF-7 cells that were not treated with any EGFR siRNA vector is set as 100%.

In this context, it can be concluded that the moderate apoptosis rate of 11.84% (Fig. 9f) achieved by EGFR siRNA formulated with GNP-PAH-3, well balances the cytotoxicity of the (EGFR siRNA)-PAH complex and the apoptosis induced by EGFR siRNA, leading to improved *in vitro* performance in silencing the EGFR gene expression in comparison with its control formed by Lipofectamine 2000 and EGFR siRNA (Fig. 9e).

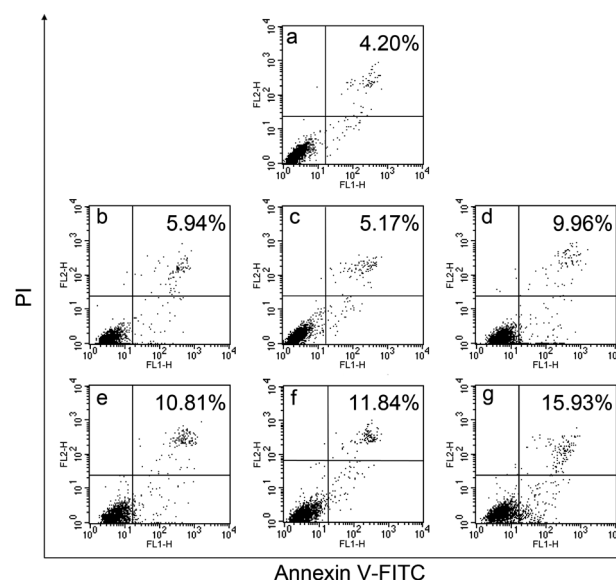


**Fig. 9** Apoptosis rates of MCF-7 cells treated with no siRNA (a), and NC siRNA loaded by Lipofectamine 2000 (b), GNP-PAH-3 (c), and PAH (d), respectively, together with those recorded from the cells treated with EGFR siRNA delivered by Lipofectamine (e), GNP-PAH-3 (f), and PAH (g), respectively.

## Conclusions

In summary, GNPs were prepared and used as a nanocarrier for constructing siRNA vectors through alternate depositions of PAH and siRNA on the particle surface. It was demonstrated that the surface coating of the denatured BSA enables the GNPs to survive the self-assembly process through the enhanced colloidal stability. The ionic LbL self-assembly method offers the effective measure not only for loading siRNA, but also for finely tuning the surface potential of the resultant GNP-PAH vectors, which consequently allows the following investigations on the surface potential-dependent cytotoxicity and cellular uptake behavior of the GNP vectors. The confocal fluorescence microscopy studies reveal that the GNP-PAH vectors with a surface potential of  $\sim +25$  mV possess superior endosomal/lysosomal escaping capacity in comparison with the particulate vectors constructed by GNP and PDDA, suggesting that the proton-sponge effect observed from PEI is also applicable for PAH. Further EGFR gene silencing investigations reveal that the GNP-PAH vector loaded with EGFR siRNA can specifically inhibit the EGFR expression in the human breast cancer MCF-7 cells *in vitro*, almost by the same level as that achieved by the GNP-PEI vector. The flow cytometric analysis on the apoptosis of MCF-7 cells induced by EGFR siRNA suggests that the toxicity of PAH is greatly suppressed after being assembled on the surface of GNPs. Moreover, the GNP-PAH presents improved EGFR silencing efficacy in comparison with the commercial transfection reagent Lipofectamine 2000, which therefore makes the GNP-PAH vectors potentially useful for more efficient *in vitro* gene delivery.

## Acknowledgements

This work was jointly supported by NSFC projects (20903100, 81072597, 81090271), the National Basic Research Program of China (2007CB935801, 2009CB930300, 2011CB935800), and the Beijing NSF project (7112089).

## Notes and references

- G. J. Hannon, *Nature*, 2002, **418**, 244–251.
- A. Fire, S. Xu, M. K. Montgomery, S. A. Kostas, S. E. Driver and C. C. Mello, *Nature*, 1998, **391**, 806–811.
- S. M. Elbashir, J. Harborth, W. Lendeckel, A. Yalcin, K. Weber and T. Tuschl, *Nature*, 2001, **411**, 494–498.
- M. Jiang and J. Milner, *Oncogene*, 2002, **21**, 6041–6048.
- D. W. Sah, *Life Sci.*, 2006, **79**, 1773–1780.
- Y. K. Oh and T. G. Park, *Adv. Drug Delivery Rev.*, 2009, **61**, 850–862.
- J. Soutschek, A. Akinc, B. Bramlage, K. Charisse, R. Constien, M. Donoghue, S. Elbashir, A. Geick, P. Hadwiger, J. Harborth, M. John, V. Kesavan, G. Lavine, R. K. Pandey, T. Racie, K. G. Rajeev, I. Rohl, I. Toudjarska, G. Wang, S. Wuschko, D. Bumcrot, V. Koteliansky, S. Limmer, M. Manoharan and H. P. Vornlocher, *Nature*, 2004, **432**, 173–178.
- M. A. Kay, J. C. Glorioso and L. Naldini, *Nat. Med.*, 2001, **7**, 33–40.
- W. Walther and U. Stein, *Drugs*, 2000, **60**, 249–271.
- M. E. Davis, *Curr. Opin. Biotechnol.*, 2002, **13**, 128–131.
- P. Ghosh, G. Han, M. De, C. K. Kim and V. M. Rotello, *Adv. Drug Delivery Rev.*, 2008, **60**, 1307–1315.
- P. S. Ghosh, C. K. Kim, G. Han, N. S. Forbes and V. M. Rotello, *ACS Nano*, 2008, **2**, 2213–2218.
- A. Elbakry, A. Zaky, R. Liebl, R. Rachel, A. Goepferich and M. Breunig, *Nano Lett.*, 2009, **9**, 2059–2064.
- D. A. Giljohann, D. S. Seferos, A. E. Prigodich, P. C. Patel and C. A. Mirkin, *J. Am. Chem. Soc.*, 2009, **131**, 2072–2073.
- J. S. Lee, J. J. Green, K. T. Love, J. Sunshine, R. Langer and D. G. Anderson, *Nano Lett.*, 2009, **9**, 2402–2406.
- D. A. Giljohann, D. S. Seferos, W. L. Daniel, M. D. Massich, P. C. Patel and C. A. Mirkin, *Angew. Chem., Int. Ed.*, 2010, **49**, 3280–3294.
- S. Guo, Y. Huang, Q. Jiang, Y. Sun, L. Deng, Z. Liang, Q. Du, J. Xing, Y. Zhao, P. C. Wang, A. Dong and X. J. Liang, *ACS Nano*, 2010, **4**, 5505–5511.
- J. H. Lee, K. Lee, S. H. Moon, Y. Lee, T. G. Park and J. Cheon, *Angew. Chem., Int. Ed.*, 2009, **48**, 4174–4179.
- H. Duan and S. Nie, *J. Am. Chem. Soc.*, 2007, **129**, 3333–3338.
- M. V. Yezhelyev, L. Qi, R. M. O'Regan, S. Nie and X. Gao, *J. Am. Chem. Soc.*, 2008, **130**, 9006–9012.
- J. Jung, A. Solanki, K. A. Memoli, K. Kamei, H. Kim, M. A. Drahl, L. J. Williams, H. R. Tseng and K. Lee, *Angew. Chem., Int. Ed.*, 2010, **49**, 103–107.
- Y. Li, X. Duan, L. Jing, C. Yang, R. Qiao and M. Gao, *Biomaterials*, 2011, **32**, 1923–1931.
- M. C. Daniel and D. Astruc, *Chem. Rev.*, 2004, **104**, 293–346.
- E. E. Connor, J. Mwamuka, A. Gole, C. J. Murphy and M. D. Wyatt, *Small*, 2005, **1**, 325–327.
- X. Huang, P. K. Jain, I. H. El-Sayed and M. A. El-Sayed, *Nanomedicine*, 2007, **2**, 681–693.
- G. Sonavane, K. Tomoda and K. Makino, *Colloids Surf., B*, 2008, **66**, 274–280.
- Z. T. Li, Z. N. Zhu, W. J. Liu, Y. L. Zhou, B. Han, Y. Gao and Z. Y. Tang, *J. Am. Chem. Soc.*, 2012, **134**, 3322–3325.
- B. Qin, H. Y. Chen, H. Liang, L. Fu, X. F. Liu, X. H. Qiu, S. Q. Liu, R. Song and Z. Y. Tang, *J. Am. Chem. Soc.*, 2010, **132**, 2886–2888.
- M. Y. Gao, B. Richter, S. Kirstein and H. Möhwald, *J. Phys. Chem. B*, 1998, **102**, 4096–4103.
- M. Y. Gao, B. Richter and S. Kirstein, *Adv. Mater.*, 1997, **9**, 802.
- Z. Z. Zheng, X. Y. Li, Z. F. Dai, S. Q. Liu and Z. Y. Tang, *J. Mater. Chem.*, 2011, **21**, 16955–16962.
- O. Boussif, F. Lezoualc'h, M. A. Zanta, M. D. Mergny, D. Scherman, B. Demeneix and J. P. Behr, *Proc. Natl. Acad. Sci. U. S. A.*, 1995, **92**, 7297–7301.
- W. J. Song, J. Z. Du, T. M. Sun, P. Z. Zhang and J. Wang, *Small*, 2010, **6**, 239–246.
- Q. Wang, Y. C. Kuo, Y. W. Wang, G. Shin, C. Ruengruglikit and Q. R. Huang, *J. Phys. Chem. B*, 2006, **110**, 16860–16866.
- V. Vichai and K. Kirtikara, *Nat. Protoc.*, 2006, **1**, 1112–1116.
- A. Akinc, M. Thomas, A. M. Klibanov and R. Langer, *J. Gene Med.*, 2005, **7**, 657–663.
- R. I. Nicholson, J. M. Gee and M. E. Harper, *Eur. J. Cancer*, 2001, **37**(suppl 4), S9–S15.
- H. E. Jones, J. M. Gee, I. R. Hutcheson, J. M. Knowlden, D. Barrow and R. I. Nicholson, *Endocr. Relat. Cancer*, 2006, **13**(suppl 1), S45–S51.
- M. Zhang, X. Zhang, C. X. Bai, J. Chen and M. Q. Wei, *Acta Pharmacol. Sin.*, 2004, **25**, 61–67.
- Q. W. Fan and W. A. Weiss, *Oncogene*, 2005, **24**, 829–837.
- H. Nozawa, T. Tadakuma, T. Ono, M. Sato, S. Hiroi, K. Masumoto and Y. Sato, *Cancer Sci.*, 2006, **97**, 1115–1124.
- C. S. Kang, Z. Y. Zhang, Z. F. Jia, G. X. Wang, M. Z. Qiu, H. X. Zhou, S. Z. Yu, J. Chang, H. Jiang and P. Y. Pu, *Cancer Gene Ther.*, 2006, **13**, 530–538.